CHAPTER 3

Evaluating the Impacts of Carbonaceous Aerosols on Clouds and Climate

Surabi Menon[1,2] and Anthony D. Del Genio[3]

[1]Lawrence Berkeley National Laboratory, Berkeley, CA

[2]Also at NASA Goddard Institute for Space Studies/Columbia University, New York, NY

[3]NASA Goddard Institute for Space Studies, New York, NY

3.1 Introduction

Any attempt to reconcile observed surface temperature changes within the last 150 years to changes simulated by climate models that include various atmospheric forcings is sensitive to the changes attributed to aerosols and aerosol-cloud-climate interactions, which are the main contributors that may well balance the positive forcings associated with greenhouse gases, absorbing aerosols, ozone related changes, etc. These aerosol effects on climate, from various modeling studies discussed in Menon (2004), range from +0.8 to -2.4 W m^{-2}, with an implied value of -1.0 W m^{-2} (range from -0.5 to –4.5 W m^{-2}) for the aerosol indirect effects. Quantifying the contribution of aerosols and aerosol-cloud interactions remain complicated for several reasons some of which are related to aerosol distributions and some to the processes used to represent their effects on clouds. Aerosol effects on low lying marine stratocumulus clouds that cover much of the Earth's surface (about 70%) have been the focus of most of prior aerosol–cloud interaction effect simulations. Since cumulus clouds (shallow and deep convective) are short lived and cover about 15 to 20% of the Earth's surface, they are not usually considered as radiatively important. However, the large amount of latent heat released from convective towers, and corresponding changes in precipitation, especially in biomass regions due to convective heating effects (Graf et al. 2004), suggest that these cloud systems and aerosol effects on them, must be examined more closely. The radiative heating effects for mature deep convective systems can account for 10-30% of maximum latent heating effects and thus cannot be ignored (Jensen and Del Genio 2003). The first study that isolated the sensitivity of cumulus clouds to

aerosols was from Nober et al. (2003) who found a reduction in precipitation in biomass burning regions and shifts in circulation patterns. Aerosol effects on convection have been included in other models as well (cf. Jacobson, 2002) but the relative impacts on convective and stratiform processes were not separated. Other changes to atmospheric stability and thermodynamical quantities due to aerosol absorption are also known to be important in modifying cloud macro/micro properties. Linkages between convection and boreal biomass burning can also impact the upper troposphere and lower stratosphere, radiation and cloud microphysical properties via transport of tropospheric aerosols to the lower stratosphere during extreme convection (Fromm and Servranckx 2003). Relevant questions regarding the impact of biomass aerosols on convective cloud properties include the effects of vertical transport of aerosols, spatial and temporal distribution of rainfall, vertical shift in latent heat release, phase shift of precipitation, circulation and their impacts on radiation.

Over land surfaces, a decrease in surface shortwave radiation (~ 3-6 W m^{-2} per decade) has been observed between 1960 to 1990, whereas, increases of 0.4 K in land temperature during the same period that occurred have resulted in speculations that evaporation and precipitation should also have decreased (Wild et al. 2004). However, precipitation records for the same period over land do not indicate any significant trend (Beck et al. 2005). The changes in precipitation are thought to be related to increased moisture advection from the oceans (Wild et al. 2004), which may well have some contributions from aerosol-radiation-convection coupling that could modify circulation patterns and hence moisture advection in specific regions.

Other important aspects of aerosol effects, besides the direct, semi-direct, microphysical and thermodynamical impacts include alteration of surface albedos, especially snow and ice covered surfaces, due to absorbing aerosols. These effects are uncertain (Jacobson, 2004) but may produce as much as 0.3 W m^{-2} forcing in the Northern hemisphere that could contribute to melting of ice and permafrost and change in the length of the season (e.g. early arrival of Spring) (Hansen and Nazarenko, 2004). Besides the impacts of aerosols on the surface albedos in the polar regions, and the thermodynamical impacts of Arctic haze (composed of water soluble sulfates, nitrates, organic and black carbon (BC)), the dynamical response to Arctic haze (through the radiation-circulation feedbacks that cause changes in pressure patterns) is thought to have the potential to modify the mode and strength of large-scale teleconnection patterns such as the Barrents Sea Oscillation that could affect other climate regimes (mainly Europe) (Rinke et al.

2004). Additionally, via the Asian monsoon, wind patterns over the eastern Mediterranean and lower stratospheric pollution at higher latitudes (Lelieveld et al. 2002) are thought to be linked to the pollutants found in Asia, indicating the distant climate impacts of aerosols.

Thus, it becomes difficult to quantify regional changes in precipitation or radiation in the context of a regional model, since long-range transport of aerosols and its dynamical impacts can play an important role in modifying distant climates and can affect boundary conditions that are imposed in regional simulations. On the other hand the use of a global model to investigate regional changes may lead to problems associated with not resolving processes on coarse spatial scales unless one examines larger domains or processes operating on larger scales. Here, we will examine global model simulations of the indirect effect for warm clouds, both stratiform and convective, in order to examine the influence of aerosols in modifying precipitation and radiation. Since stratus clouds cover large areas spatial domain is not a constraint, and for convective clouds in biomass regions, the area covered by biomass burning may be large enough to examine regional influences. Section 2 describes the model and simulations that were performed in this study, Section 3 describes the results from the modeling study as well as results obtained for different regions, and finally in Section 4 we present the conclusions from this study.

3.2 Model Description

We use the Goddard Institute for Space Studies (GISS) ModelE, the latest version of model II' described in more detail by Schmidt et al. (2005) and Hansen et al. (2005) coupled to the aerosol chemistry model of Koch et al. (1999, 2005). Cloud water is treated prognostically in the model (Del Genio et al. 1996), with representation of sources due to large-scale convergence and cumulus detrainment and sinks due to autconversion, accretion, evaporation, and cloud top entrainment, as well as precipitation enhancement due to the seeder-feeder effect. Stratiform cloud cover is a diagnostic function of relative humidity and stability allowing for subgrid vertical cloud fraction. Moist convection uses a quasi-equilibrium cloud base closure with entraining and non-entraining updrafts and a cumulus-scale downdraft. Main changes in the updated GCM of relevance to the indirect effect include a microphysics-based cumulus scheme described in Del Genio et al. (2005) and inclusion of sub-grid turbulence at all levels of the GCM (based on the second order closure model of Cheng et al. 2003). Improvements to the cumulus

scheme include a more physical partioning of convective condensate between precipitation and detrainment into anvil clouds based on a microphysics scheme (using a Marshall-Palmer distribution for droplets, empirical droplet size - terminal velocity relationships for liquid, graupel, and ice hydrometeors and prescribed cumulus updraft speeds).

The aerosol emission data sets used in the model are derived from AEROCOM (An aerosol model intercomparison project) (Frank Dentener, personal communication, 2004). Sulfate aerosols include fossil fuel sources that are country-based emissions for the Year 2000 and both continuously erupting and explosive volcanoes (Andres and Kasgnoc, 1998, Halmer and Schmincke, 2003) as well as dimethyl sulfide emissions. Carbonaceous aerosols (treatment described in Koch and Hansen, 2005) include fossil- and biofuel sources from Bond et al. (2004) and biomass sources. Biomass sources for sulfates and carbonaceous aerosols are from Van der Werf et al. (2004). In addition, organic aerosols include a fraction of natural terpenes (15%) from secondary organics. Solubility for industrial carbonaceous aerosols is 100% for aged aerosols (e-folding time of 1 day) and for the biomass components solubilities of 80% and 60% are assumed for organic and BC, respectively. Sea-salt is also calculated based on model wind speeds (Koch et al. 2006) instead of through the source function used previously (Koch et al. 1999). All aerosols are treated as external mixtures, which may not accurately represent aerosol radiative properties for regions away from sources, where aerosols tend to form internal mixtures.

Improvements to the treatment of the aerosol indirect effect described in Menon et al. (2002a) (hereafter referred to as M02) include a semi-prognostic treatment of the cloud droplet number concentration (CDNC), addition of BC aerosol effects on clouds, and incorporation of sub-grid vertical velocity effects on cloud droplet number. Several parameterizations have been used to determine CDNC, which is the main and critical link between the aerosols and cloud microphysics. The resulting values for the indirect effect vary by ~ 40%, depending on the assumptions or parameterizations used. Kiehl et al. (2000) find over a factor of three difference in their estimate of the indirect effect when using different CDNC schemes. Here, we mainly refer to simulations which uses the parameterization from Gultepe and Isaac (1999), given as:

$$\begin{aligned} CDNC_{Land} &= 298 \times \log_{10} Na_{Land} - 595 \\ CDNC_{Ocean} &= 162 \times \log_{10} Na_{Ocean} - 273 \end{aligned} \qquad (3.1)$$

where N_a is the aerosol concentration (cm^{-3}) calculated from the aerosol mass concentration and assumed sizes as used in Lohmann et al. (1999). N_a for land include the effects of sulfates, organic and BC aerosols, whereas, N_a for ocean includes, in addition, sea-salt aerosols. The values so derived for CDNC are representative of in-cloud CDNC values since measurements were for in-cloud values. Dust is assumed to be insoluble in these simulations and since the amount of dust roughly remains unchanged for present-day and pre-industrial simulations, its contribution to the indirect effect in terms of changes in CDNC are neglected. Future treatments will include dust formed on sulfate or sea-salt via heterogeneous chemical reactions (Bauer et al. 2005), which is not discussed in this work. Aerosol sources for present-day simulations include both anthropogenic (sulfates and carbonaceous aerosols from fossil fuel, bio fuel and biomass sources) and natural sources from dimethyl sulfide, volcanic and biomass emissions (assumed to be 50% of the anthropogenic biomass source), organic aerosols from terpenes, sea-salt and dust. Aerosol sources for pre-industrial simulations include just the natural sources. Where applicable, we use "Δ" to denote differences between present-day and pre-industrial simulations. All simulations use fixed sea-surface temperatures derived for present-day climatologies. All results reported are based on six years of model simulations averaged over the last five years.

3.3 Aerosol Indirect Effect on Warm Clouds

Prior model estimates of the aerosol indirect effect with the GISS GCM (M02) are based on simulations that distinguish between pre-industrial and present-day aerosol emissions. These estimates were found to be dependent on the background concentration imposed for either aerosols or CDNC. As an example, in climate simulations for present-day versus pre-industrial aerosols, changing the minimum (background) CDNC from 10 to 40 cm^{-3} produces a decrease of almost 50% in the indirect effect estimate (Menon 2004). Here, we use a value of 20 cm^{-3} for background CDNC for all our simulations based on surface observations that indicate values of ~10 to 20 cm^{-3} in pure marine background air with no wind (J.-L. Brenguier, personal communication). We perform several sets of simulations, shown in Table 3.1, to investigate the impacts of fossil- and biofuel BC aerosols, aerosol-convective cloud effects, and the semi-direct aerosol effects. Note that all simulations only include aerosol effects on warm cloud microphysics and include both the first indirect effect (changes in cloud reflectivity due to smaller droplet sizes) (Twomey, 1977) and the second indirect effect (changes in cloud lifetime

and cloud cover from suppression of precipitation) (Albrecht, 1989). Our indirect effect represents the net effects of aerosols on clouds since it includes implicit changes to cloud fields from other climate feedbacks.

Additional simulations similar to those listed in Table 3.1 were performed that include aerosol emissions for pre-industrial scenarios (Year 1850). Present-day emissions (Year 2000) include both natural and anthropogenic aerosols. Most of the treatment for the aerosol indirect effect follows that given in M02, except that we modulate the CDNC so that it changes with cloud cover and cloud water changes. Here, we use the formula of Beheng (1994) for autoconversion (process that initiates the conversion of cloud water to precipitation), which is a function of cloud liquid water content and CDNC. The magnitude of the indirect effect, calculated as difference between present day and pre-industrial simulations, for Exp A is ~ −1.36 W m^{-2} obtained from differences between net radiation at the top of the atmosphere (TOA) and the direct aerosol effect.

Alternatively, the aerosol indirect effect can also be obtained from the difference in net cloud radiative forcing, which then is –0.65 W m^{-2}. Differences between these methods of estimating the indirect effect, which are both approximate, are discussed in M02, and are dependent on the treatment used to separate radiation as that due to aerosols or that due to clouds. These values are significantly lower than our previous estimates which ranged from –1.55 to –4.4 W m^{-2} for the indirect effect (change in net cloud forcing) and could be attributed to the minimum CDNC used here (as opposed to 10 cm^{-3} in M02); inclusion of dust and BC aerosols (that will increase the positive forcing); inclusion of a relative humidity factor that accounts for changes in extinction efficiencies due to aerosol growth (~36% increase in net cloud forcing); choice of autoconversion parameterization and other general improvements in ModelE (e.g.: improvements to the convective scheme results in increased coverage of marine stratus clouds along the western edges of the continent, that were previously deficient (Del Genio et al. 2005)). Perhaps the more significant reason for the smaller values of the indirect effect that we obtain here is the smaller anthropogenic aerosol burden and the larger assumed natural aerosol burden (increased biomass aerosols assumed for pre-industrial conditions compared to Koch et al. 1999) as shown in Table 3.2. In Exp A the anthropogenic aerosol column burden is 2.3 times the assumed natural burden; in M02 they were 4.6 to 6.5 times the natural aerosol burden. This smaller burden leads to the large reduction in the aerosol indirect effect magnitude.

As a sensitivity test, we performed an additional simulation, similar to Exp A but with increased anthropogenic sulfates (factor of 2 increase) for present-day conditions and one with reduced biomass aerosols (10% of present-day) for pre-industrial conditions (Exp A_S). The resulting anthropogenic column burden in Exp A_S is higher by a factor of 7 compared to the assumed natural burden. Compared to ΔExp A, the magnitude of the indirect effect increases by 60% for ΔExp A_S, mainly due to the higher anthropogenic burden in Exp A_S. As shown in Table 3.2, in addition to the choice of the autoconversion parameterization (which leads to some of the differences in the two M02 simulations), aerosol burdens play a major role in determining changes in radiative forcing.

3.3.1 *Black Carbon Aerosol Effects on Clouds*

As shown in Table 3.3, the forcing efficiency, defined as the ratio of direct forcing to anthropogenic column burden, of fossil- and biofuel BC is quite high. Since the heating associated with these absorbing aerosols can lead to significant changes in surface energy budgets, precipitation, cloud cover and circulation (Ramanathan et al. 2001, Chung et al. 2002, Menon et al. 2002b), and since the sources for fossil- and biofuel BC may be controlled more readily (via controls on technology, e.g.: emission filters for transportation, clean-coal burning technology, use of natural gas to replace bio fuels, etc.) than that for biomass derived aerosols, a closer inspection is warranted to understand the impacts of these absorbing aerosols on clouds and climate.

Present day climate simulations with twice the BC from fossil- and biofuel sources (Exp 2BC) versus those with the standard amount (Exp A) and without any fossil- and biofuel BC (Exp NBC) were compared to climate simulations with pre-industrial aerosol concentrations. For annual global changes, major differences were decreased net radiation (solar) at the surface, decreased sensible heat flux, precipitation and soil evaporation for increasing amounts of BC. Increases in net TOA radiation, short wave cloud forcing and water cloud optical depth were also observed for increasing BC amounts. These changes; w.r.t. pre-industrial aerosol concentrations; were within 2.5% except for changes to water cloud optical depths (>10%), net TOA radiation (>15%) and net heating (>15%) at the surface. Differences of 3% are also manifested in cloud top temperature (which decreases with increasing BC) for varying BC amounts. While global differences are not as high, regional changes are more significant and are discussed in more

detail in Sec. 3.3.3.1. Although changes in optical depth are related to changes in cloud water paths and cloud droplet sizes, the increase in cloud optical depth is not related to changes in CDNC (~ 5% between Exp A, 2BC and NBC), but rather to changes due to the thermodynamical effects of heating (sensible and latent heat fluxes) that changes the availability of water since precipitation is reduced.

Also of significance are changes to the zonally averaged vertical profiles of temperature at higher latitudes, that increase with increasing BC especially towards the poles and higher levels (indicative of upper tropospheric transport of warm air), and solar radiation heating rates that are much stronger in the Northern Hemisphere. This is not surprising since impacts of BC related forcing tends to be stronger in regions of high surface albedo (Hansen and Nazarenko, 2004). Increasing amounts of BC also leads to greater reduction in the extent of snow and ice cover (reduction in ΔExp 2BC and ΔExp A are a factor of 1.6 compared to ΔExp NBC) as was also indicated by Hansen and Nazarenko (2004), Wang (2004) and Roberts and Jones (2004); with stronger changes in the Northern hemisphere and the Arctic than in the Antarctic. Also of significance is the change in sea-level pressure over all ocean regions and part of the NH continents (positive anomalies in ΔExp 2BC replace neutral changes found in ΔExp A and ΔExp NBC) indicative of changes in the circulation patterns that are stronger in ΔExp 2BC. Similar to the results of Wang (2004) we find changes in circulation and snow cover, as well as surface fluxes with changing BC amounts. Analyses of the June to August precipitation fields for Exp A, NBC and 2BC, does indicate a northward shift in the intertropical convergence zone (ITCZ) in Exp 2BC and Exp A as was also observed in simulations of BC climate effects by Wang (2004) and Roberts and Jones (2004). Without fossil- and biofuel BC this northward shift in the ITCZ is not evident.

Other uncertainties, besides vertical and horizontal distributions, are related to absorption properties of BC within clouds. In-cloud absorption by BC is thought to increase the absorption efficiency of clouds by 5% globally, with more significant regional changes (15-25%) (Chuang et al. 2002). These results were for the first indirect effect only. Accounting for these BC absorption effects in cloud, for both indirect effects; via a proxy enhancement factor (25%) that is analogous to increasing BC optical depth, results in a 12% increase in net cloud forcing (sum of shortwave and longwave) globally. Regionally, differences are much greater in regions with large BC emissions and co-located clouds. In terms of surface temperature response with BC in-

cloud heating included, as shown in Figure 3.1, global differences are negligible but regional differences are much greater in regions where BC emissions dominate such as Asia, Europe and eastern US. Note that these responses are mainly a sensitivity test to indicate the lower bound of the change in temperature when BC in-cloud absorption in accounted for, since we use an atmosphere-only model with prescribed sea surface temperatures (Wang, 2004). A coupled ocean-atmosphere model would be more effective in simulating the full impact of observed surface temperature changes.

In an atmosphere model (Hadley Center climate model) coupled to a slab ocean model with four times as much fossil fuel BC as in Exp A, annual mean surface temperature change is ~ 0.436K giving a climate sensitivity of 0.56 K W^{-1} m^2 (Roberts and Jones, 2004). However, effects of BC on cloud properties are not explicitly parameterized in these simulations. Within the same model the climate sensitivity to doubled CO_2 is about 0.91 K W^{-1} m^2. Another study on temperature response per unit of direct forcing (Jacobson, 2002), without the use of a slab-ocean model, reports a value of 1.4 K W^{-1} m^2 for BC and OC from fossil fuel. While a direct comparison to these values are not possible in the context of our simulations (since they include different methods on treatment of carbon optics and climate effects), we can compare the ratios of the relative magnitude of surface temperature changes to radiative flux values between ΔExp A, ΔExp NBC and ΔExp 2BC. These simulations mainly differ in terms of the amounts of fossil- and biofuel BC. The values for ΔExp A, ΔExp NBC and ΔExp 2BC are 0.12, 0.097, and 1.14 K W^{-1} m^2, respectively. The sensitivity of this version of the model coupled to a mixed ocean slab model to doubled CO_2 is ~0.66 K W^{-1} m^2 (Hansen et al. 2005). Although we cannot directly compare between these BC and CO_2 related climate changes from the GISS GCM, since a coupled ocean-atmosphere model must be used to accurately estimate the climate sensitivity to BC, results from Roberts and Jones (2004) and Hansen et al. (2005) do suggest that climate sensitivity factors for BC may be quite comparable to that of CO_2.

3.3.2 *Aerosol effects on Convective Clouds*

Besides the radiative effects of fossil- and biofuel aerosols, aerosol effects from biomass burning are also important especially near regions that are more active convectively. Here we examine aerosol effects on convective clouds, in addition to stratiform clouds. Since parameterizations for predicting CDNC from aerosols for convective clouds are not as well developed as that for

stratiform clouds, we use the same droplet prediction scheme for convective clouds as for stratiform clouds (Exp CC1), following the approach of Nober et al. (2003). Similar to Nober et al. (2003) and based on empirical data from Lahav and Rosenfeld (2000) we modify the precipitation rate as a function of cloud base CDNC and temperature, such that for temperatures below 263K and for low CDNC values (<750 cm^{-3}), precipitation remains unchanged; and with increasing CDNC and temperatures above 263K precipitation reduces to 25% (750 cm^{-3} < CDNC <1000 cm^{-3}) and 0% (CDNC >1000 cm^{-3}), respectively. These simulations only account for aerosol effects on warm convective clouds. The suppression of rain in warm convective clouds should lead to increased water contents and therefore should also have an effect on freezing rates for cold clouds and precipitation changes (Andreae et al. 2004) via the Bergeron-Findeisen process, which facilitates ice-phase precipitation processes at the expense of warm-phase processes.

In addition to Exp CC1, we conducted a second simulation (Exp CC2) with CDNC based on observations from the Cirrus Regional Study of Tropical Anvils – Florida Area Cirrus Experiment (CRYSTAL FACE) data for warm cumulus clouds (Conant et al. 2004). The relationship we use is given as:

$$CDNC = 10^{[0.433+0.815\log N_a + 0.280\log(w)]} \tag{3.2}$$

Here, w is the updraft velocity in m s^{-1}. Since model diagnostics do not account for cloud-scale updraft velocities we use the following notation

$$w = \overline{w} + \sqrt{0.66 \times TKE} \tag{3.3}$$

where $\overline{w}$ is the grid average updraft velocity and TKE is the turbulent kinetic energy (Ye Cheng, personal communication). Most of the climate diagnostics for ΔExp CC2 are similar to those for ΔExp CC1 except for larger differences in the net radiation at TOA, cloud water optical depths, and net heating at the surface, leading to differences in soil evaporation, sensible heat flux, precipitation. Larger differences are seen regionally and are discussed in Sec. 3.3.3.2.

Changes with the addition of aerosol-convective cloud effects (Exp CC1/CC2 versus Exp A) include increases in the liquid water path (40%), water and ice cloud optical depths (20% and

over a factor of 2 increase, respectively), net TOA radiation and net ground heating (70% decrease), shortwave (16%) and longwave (7%) cloud forcing. Increase in cloud cover (water or ice, convective or total) is less than 5% and reduction in total precipitation is between 2 to 10%. With the increase in cloud water (almost a factor of 2), effective water cloud particle sizes (product of cloud effective radii and optical depth) are ~50% larger. More importantly, with aerosol-convective cloud effects level of precipitation formation may be shifted higher since most of the cloud water increase is at higher levels. Shifts from warm to cold precipitation processes should increase the height at which latent heat is released in clouds with similar rainfall amounts as well as increase the water available for ice processes, lightning and more intense convective storms (Andreae et al. 2004).

Changes in aerosol concentration for present-day versus pre-industrial simulations (higher by a factor of 2.7) results in values of 0 and 0.22 W m^{-2} for the indirect effect from changes in net cloud radiative forcing for ΔExp CC1 and ΔExp CC2, respectively and –0.43 W m^{-2} for both ΔExp CC1 and ΔExp CC2 when accounting for the difference in Net TOA radiation and the direct effect. Despite similar increases in aerosol burdens, between ΔExp CC1, ΔExp CC2 and ΔExp A, this reduction in the net cloud radiative forcing obtained when including aerosol-convective cloud effects may arise from changes in the longwave component that are somewhat comparable to the shortwave. Some differences may also arise from changes in aerosol burden as indicated from a sensitivity test conducted to understand changes in climate diagnostics for differences in biomass aerosols. At present, we assume that pre-industrial biomass aerosols are ~ 50% of present-day biomass emissions. These estimates are highly uncertain since separating natural and anthropogenic contributions to biomass burning over the last 150 years is subject to a lot of uncertainty (Dorothy Koch, personal communication). Thus, we perform similar simulations as Exp CC2 but with 10% of biomass for pre-industrial simulations. As compared to ΔExp CC2 the aerosol indirect effect is now slightly negative (–0.07 W m^{-2}).

Nober et al. (2003) find no significant signal in the radiation budgets in their simulations, though it is not clear if they refer to changes between simulations with and without aerosol-convective cloud effects or changes with respect to changing aerosol concentrations. In our case, we do find increased cloud radiative forcings (more negative) for Exp CC1 and CC2 compared to Exp A, and smaller cloud radiative forcings for ΔExp CC1 and ΔExp CC2 compared to ΔExp

A. Although aerosol-convective cloud effects may appear to be radiatively unimportant in the simulations of Nober et al. (2003) they do find a weakening of the Walker circulation during June to August caused by the negative precipitation anomaly of the summer monsoon over the Indian subcontinent and surrounding regions including the Southwest Pacific, which are correlated to changes in the velocity potential fields. In our simulations, zonally averaged profiles of vertical velocity and vertical transport of latent heat for June to August indicate increased vertical velocities and increased vertical transport of latent heat in the Southern Tropics for Exp CC1/CC2 versus Exp A, along with increased water contents at higher atmospheric levels. Comparison of observed June-July-August precipitation fields (e.g. from the global precipitation climatology project, http://precip.gsfc.nasa.gov/gifs/sg_v2.0259.gif) with present day simulations for Exp A, CC1 and CC2 (Figure 3.3a) indicate that Exp CC2 may exaggerate the reduction in precipitation in the Amazonia, but Exp CC1 does simulate the precipitation amounts over the tropical convective regions and the mid eastern Amazonia a bit more realistically than Exp A. This can be seen in Figure 3.3b, which shows the difference in precipitation between Exp CC1 and Exp A (The decrease and increase in precipitation over the biomass burning regions are in the same direction as observations).

3.3.3 *Regional Impacts of Aerosols on Clouds and Climate*

Changes in global annual values may obscure significant regional as well as seasonal changes from manifesting itself. Thus, it becomes necessary to focus on regional changes within a global model since although aerosol sources vary regionally, transport and teleconnections may play a role in modifying climate at a distant. Such changes have been found in several other studies that investigated the role of Asian and European/Russian aerosols in affecting the distant Arctic climate (Koch and Hansen 2005), and increases in aerosol concentrations in North America via transport of dust plumes (that include entrained pollutants) from Mongolia and China (DeBell et al. 2004) have also been observed. Seasonality can also play a strong role in the types of aerosols that are produced (fossil or biomass based production) and thus may change values of the resulting radiative fluxes (Menon 2004). Here, we focus on those regions that have the largest changes in either biomass or fossil- and biofuel based aerosols. The seasons are chosen based on the availability of observations from large field campaigns so that model simulations of certain variables may be compared to observed values.

3.3.3.1 *Black Carbon Aerosol Effects on Regional Climate*

Aerosol effects over China are thought to be partly responsible for the anomalous changes in the precipitation field observed over the last 30 years, with the north being more prone to droughts, while the south is subject to large-scale flooding (Xu 2001, Menon et al. 2002b). Several other studies have investigated changes in sunshine duration, diurnal cycle of temperature, and in the anomalies of the northwestern Pacific subtropical high, (Kaiser and Qian, 2002; Gong et al. 2004), which are correlated to these anomalous precipitation fields. Similarly, over the Indian subcontinent and surrounding regions, Ramanthan et al. (2001) and Chung et al. (2002) find large spatial changes in the distribution of precipitation related to changes in surface forcing, from absorbing aerosols.

Here, we show values of radiative fluxes at the surface, TOA and the atmospheric column along with precipitation for select regions over India and China in Tables 3.4a and 3.4b, respectively. The region over China was based on prior results from Menon et al. (2002b) and Menon (2004) to highlight changes in the northern/southern regions based on changes due to BC. Over India, we chose a region based on field data that were available from the Indian Ocean Experiment (INDOEX) as given in Ramanathan et al. (2001). During January to March of 1999, radiative forcings at the surface, TOA and the atmospheric column were –20, –2, 18 W m^{-2} for the direct aerosol effect and –6, –5, 1 W m^{-2} when including the 1st aerosol indirect effect (Ramanathan et al. 2001). Values as high as 33 W m^{-2} have been reported based on observed radiative fluxes and aerosol properties at a site in India during the dry season (January-April) (Pandithurai et al. 2004) for the aerosol direct effect. In our simulations, the forcings computed for the Indian subcontinent and Ocean region for the January-March period, shown in Table 3.4a are for differences between present-day and pre-industrial aerosol emissions, similar to those from Ramanathan et al. (2001). As shown in Table 3.4a, our TOA and atmospheric column fluxes are generally higher than those obtained from INDOEX. In both regions, precipitation appears to increase with increasing atmospheric fluxes (reduced surface fluxes), which may be partly due to the response of convection to the atmospheric heating, although it is not that easily demonstrated without separating it from the feedbacks that exist when linking the dynamical response of convection to heating or stability conditions as shown in Chung et al. (2002). Over China, precipitation decreases more in the north than in the south, consistent with changes in the

atmospheric fluxes for each of the simulations, though there is no direct relationship between them across the north and south domain. This suggests that along with the atmospheric aerosol content, surface and meteorological conditions also play an important role in modifying the response of precipitation to atmospheric heating.

Other climate aspects of absorbing aerosols are the direct heating effects on cloud cover- also called the "semi-direct effect" (Hansen et al. 1997). Although the semi-direct effect (calculated as the difference between TOA net irradiance for simulations with and without aerosols, due to changes in cloud fields) (Johnson et al. 2004) may be associated with positive forcing (due to changes in cloud cover that can increase the absorbed shortwave), recent studies have suggested that the sign may be dependent on the vertical aerosol distribution. In Tables 3.5a and 3.5b we show results from a large eddy scale model (Johnson et al. 2004), and a GCM based study (Menon 2004) that investigated regional forcings associated with different vertical distributions of absorbing aerosols. As shown in Table 3.5a, with absorbing aerosols above the boundary layer, the semi-direct effect can be negative, mainly due to the increases in liquid water path (LWP) fields and entrainment effects that led to a shallower moister boundary layer with higher LWP (Johnson et al. 2004). In the GCM study, the effects of vertical velocity, that got stronger as aerosols were distributed higher, led to increased cloud formation and LWP, that in turn changed the semi-direct effect from positive to negative (Menon 2004). Penner et al. (2003) also find negative semi-direct effects for biomass aerosols injected in the mid troposphere, mainly by accounting for the longwave forcing (longwave forcing decreases when high cloud cover decreases).

On a global average, the semi-direct effect, as indicated in a simulation comparable to Exp A, but without including the indirect aerosol effects (CDNC is kept a constant at 174 cm^{-3} for land and ~60 cm^{-3} for ocean), is ~ –0.08 W m^{-2}. Regions of negative values are co-located with high biomass burning regions, and changes to both longwave cloud radiative forcing and high cloud cover are negative compared to ΔExp A. Thus, these negative longwave effects outweigh the positive forcings due to cloud reduction, that then result in a semi-direct effect that is negative in regions of strong biomass burning. However, Koren et al. (2004) find that for heavy smoke conditions in the Amazonia, the cumulus cloud cover decreases by 38% as compared to clean conditions, with an overall instantaneous forcing of 8 W m^{-2}. Another study in the Middle East during the Kuwait oil fires, found that depending on the stability of the atmosphere and humidity

profiles, large deep convective clouds can form at the top of the smoke layer (Rudich et al. 2003). Thus, vertical profiles of temperature (heating) (and thus of aerosols) and humidity may play a leading role in changing the sign of the semi-direct aerosol effects due to changes in cloud cover. These various results are difficult to interpret since observations of vertical aerosol distributions remain sparse.

3.3.3.2 *Effects of Biomass Aerosols over Amazonia*

During the active fire season large amounts of forests are burned in the Amazonia and changes in carbon fluxes, as well as cloud properties, are significantly different compared to the areas not affected by burning as shown from satellite records (Kaufman and Fraser, 1997). Results from a large field campaign conducted over the Amazonia during the fire season were recently obtained that indicate changes in deep convective cloud properties and precipitation when the Amazonia was separated into a green ocean (biomass source region), blue ocean (ocean) and a polluted smoky region (Andreae et al. 2004). Since we use seasonal means for August to October, specific days of active burning are not accounted for and thus, we mainly contrast values for the ocean (5N-5S, 30-40W) "blue ocean", versus regions with large biomass emissions (5-15S, 50-75W), "green ocean". Using this separation, in Figure 3.4, we compare model computations of precipitation changes for Exp A, Exp CC1 and Exp CC2 for the two regimes (blue and green ocean). Precipitation changes refer to the difference in precipitation from pre-industrial to present-day values. The bottom panel of Figure 3.4 shows CDNC values for present-day to facilitate comparison with observations. CDNC values from the SMOCC campaign (Andreae et al. 2004) are 200, 600 and 2200 cm^{-3} for the blue ocean, green ocean and for the smoky clouds, respectively. Within uncertainties that are bound to exist when comparing single point/time values with averages from the model over larger domains, the CDNC values for Exp CC1 and CC2 are more comparable to those measured than are values for Exp A.

As shown in Figure 3.4, precipitation changes from the ocean to the biomass regions are stronger for Exp CC1 and CC2 mainly due to the substantial increase in CDNC obtained for convective clouds. Without aerosol-convective cloud effects, the percentage change in precipitation is small. In addition, zonally averaged vertical profiles of particle size indicate that the size of particles needed to participate in coalescence processes (12-14 μm) is at ~900 hPa in Exp A, but in both Exp CC1 and CC2, these levels are between 600 to about 900 hPa, indicative

of a shift in onset of precipitation. Andreae et al. find a shift in the onset of precipitation under smoky conditions that tend to favor the formation of large ice hydrometeors, though the change in the amount or areal distribution of precipitation was not evident because the increased intensity of storms compensates the effects of suppression of precipitation initiation (time and level for cloud droplet sizes to reach the coalescence size) and increased intensity of storms. In ΔExp CC1 and CC2 we do find a larger decrease in precipitation (factor of 2 to over 4 for the percentage change in precipitation) from the ocean region to the biomass regions compared to the 70% decrease seen in ΔExp A. However, verification of such changes with observations is not possible and thus these values are mainly indicative of the sensitivity of precipitation to changing CDNC in convective clouds.

3.4 Conclusion

In the newly updated version of the GISS GCM, the aerosol indirect effect was found to be –0.65 W m^{-2} (or alternatively –1.36 W m^{-2}), much lower than previous values obtained in Menon et al. (2002a) that ranged from –2.4 to –4.4 W m^{-2}. These lower values were mainly due to smaller differences in the anthropogenic aerosol burdens currently assumed, changes in the aerosol extinction efficiency due to aerosol effects on relative humidity (36%), addition of BC and dust aerosols, amongst other general improvements in the updated model. Including aerosol effects on convective clouds shifts the cloud water content to higher levels, as well as changes the initiation of precipitation formation to higher levels. The percentage change in precipitation for the clean ocean regions versus the biomass regions were found to vary by a factor of 2 to 4 mainly due to the increase in cloud droplets in convective clouds. The aerosol indirect effect with aerosol-convective cloud effects included ranged from +0.22 to –0.43 W m^{-2} and was much lower than estimates without aerosol-convective cloud effects, some of which may be related to changes in the longwave cloud forcing that was of similar magnitude as the shortwave cloud forcing. The global magnitude of the aerosol semi-direct effect was found to be close to 0 (–0.08 W m^{-2}) since long wave effects of biomass aerosols (lofted higher) cancel out positive forcings from a reduction in cloud cover. Changes in the vertical profiles of temperature and humidity as well as the liquid water path can influence the sign of the semi-direct effect through changes in the cloud cover.

Several simulations were conducted to examine the effects of BC aerosols from fossil- and biofuel and carbonaceous aerosols from biomass burning. For twice the amount of fossil- and biofuel BC emissions, with all indirect effects included, the ratio of surface temperature to TOA radiative fluxes increases by more than a factor of 10 (changes from 0.097 to 1.14 K W^{-1} m^2). While the forcing associated with BC may be somewhat linear, the temperature response to the forcing is non-linear since it includes changes in cloud fields and other feedbacks. Climate sensitivity to doubled CO_2 in a similar version of the model coupled to a slab-ocean model is ~ 0.66 K W^{-1} m^2 (Hansen et al. 2005). These results and those from Roberts and Jones (2004) (climate sensitivity of 0.56 and 0.91 K W^{-1} m^2 for four times the fossil fuel BC amount and twice the CO_2), as well results based on the forcing efficiency of BC (Table 3.3) and Jacobson (2002), indicate that despite small atmospheric burdens (~0.13 mg m^{-2}) and short life-times (~3-7 days), BC aerosol emissions have a significant influence on climate. Regional changes in precipitation, examined over India and China, were found to be related to the amount of atmospheric heating, with higher atmospheric fluxes corresponding to larger changes (positive) in precipitation, though we do not discount the influence of surface and meteorological conditions that may also lead to similar changes. The changes described in this paper are for aerosol effects on warm clouds only, and to fully understand the net aerosol effects on climate, various aerosol effects on cold cloud microphysics must be included in future simulations.

ACKNOWLEDGEMENTS

We acknowledge support from the NASA Climate Modeling and Analysis Program managed by Don Anderson and Tsengdar Lee; the NASA GWEC project and the DOE ARM project. Additionally, SM acknowledges support from LBNL's LDRD project (supported by the Director, Office of Science, Office of Basic Energy Science, of the U.S. Department of Energy under Contract No. DE-AC02-05CH11231). The aerosol model used in this work was developed by Dorothy Koch who provided much of her expertise and guidance in its use as well as provided useful comments to this work. We gratefully acknowledge all her contributions to this work and also acknowledge comments/guidance on model simulations by Larissa Nazarenko.

REFERENCES

Andreae, M.O., Rosenfeld D., Artaxo, P., Costa, A.A., Franck, G.P., Longo, K.M. and Silva-Dias, M.A.F. (2004). Smoking rain clouds over the Amazon. *Science*, **303**, 1337-1342.

Andres, R.J., and Kasgnoc, A.D. (1998). A time-averaged inventory of subaerial volcanic sulfur emissions. *J. Geophys. Res.*, **103**(D19), 25251-25261.

Beck, C., Grieser, J. and Rudolf, B. (2005). A new monthly precipitation climatology for the global land areas for the period 1951 to 2000. *Clim Status Rep. 2004*, German Weather Service, Offenbach.

Beheng, K.D. (1994). A parameterization of warm cloud microphysical conversion processes. *Atmos. Res.* **33**, 193-206.

Bond T.C. et al. (2004). A technology-based global inventory of black and organic carbon emissions from combustion. *J. Geophys. Res.,* **109** (D14), No. D14203.

Cheng. Y., Canuto, V.M. and Howard, A.M. (2003). An improved model for the turbulent PBL. *J. Atmos. Sci.*, **60**, 3043-3046.

Chuang, C.C., Penner, J.E., Prospero, J.M., Grant, K.E., Rau, G.H. and Kawamoto K. (2002). Cloud susceptibility and the first aerosol indirect forcing: Sensitivity to BC and aerosol concentrations. *J. Geophys. Res.*, **107**, D21, 4564, doi:10.1029/2000JD000215.

Chung, C.E, Ramanathan, V. and Kiehl, J.T. (2002). Effects of South Asian absorbing haze on the northeast monsoon and surface-heat exchange, *J. Clim.*, **15**, 2462-76.

Conant, W. C., VanReken, T.M., Rissman, T.A., et al., (2004). Aerosol-cloud drop concentration closure in warm cumulus. *J. Geophys. Res.*, **109**, D13204, doi:10.1029/2003JD004324.

DeBell, L.J., Vozzella, M., Talbot, R.W. and Dibb, J.E. (2004). Asian dust storm events of spring 2001 and associated pollutants observed in New England by the Atmospheric Investigation, Regional Modeling, Analysis and Prediction (AIRMAP) monitoring network. *J. Geophys. Res.*, **109**, D01394, doi:10.1029/2003JD003733.

Del Genio, A.D., Yao, M.-S. and Lo, K.-W. (1996). A prognostic cloud water parameterization for global climate models. *J. Clim.,* **9,** 270-304.

Del Genio A.D., Kovari, W., Yao, M.-S. and Jonas, J. (2005). Cumulus microphysics and climate sensitivity. *J. Clim.*, **18**, 2376-2387.

Fromm, M.D. and Servranckx, R. (2003). Transport of forest fire smoke above the tropopause by supercell convection. *Geophys. Res. Lettr.*, **30**, 1542, doi:10.1029/2002GL016820.

Gong, D.-Y., Pan, Y.-Z. and Wang, J.-A. (2004). Changes in extreme daily mean temperatures in summer in eastern China during 1955-2000. *Theor. Appl. Climatol.*, **77**, 25-37.

Gultepe, I. and Isaac, G.A. (1999). Scale effects on averaging of cloud droplet and aerosols number concentrations: Observations and models. *J. Clim*, **12**, 1268-1279.

Halmer, M.M. and Schmincke, H.U. (2003). The impact of moderate-scale explosive eruptions on stratospheric gas injections. *Bull. Volcanology*, **65(6)**, 433-440.

Hansen, J., Sato, M. and Ruedy, R. (1997). Radiative forcing and climate response. *J. Geophys. Res.*, **102**, 6831-6864.

Hansen, J.E. and Nazarenko, L. (2004). Soot climate forcing via snow and ice albedos. *Proc. Natl. Acad. Sci*. **101**, 423-428.

Hansen, J.E., Sato, M., Ruedy, R., et al. (2005). Efficacy of climate forcings. *J. Geophys. Res.,* **110,** D18104, doi:10.1029/2005JD005776.

Jacobson, M.Z. (2002). Control of fossil-fuel particulate black carbon and organic matter, possibly the most effective method of slowing global warming. *J. Geophys. Res.*, **107**, (D19), 4410, doi:10.1029/2001JD001376.

Jacobson, M.Z. (2004). Climate response of fossil fuel and biofuel soot, accounting for soot's feedback to snow and sea ice albedo and emissivity. *J. Geophys. Res.,* **109**, D21201. doi:10.1029/2004JD004945.

Jensen, M. and Del Genio, A.D. (2003). Radiative and microphysical characteristics of deep convective systems in the tropical western Pacific. *J. Appl. Meteorol*., **42**, 1234-1254.

Johnson, B.T., Shine, K.P. and Forster, P.M. (2004). The semi-direct aerosol effect: Impact of absorbing aerosols on marine stratocumulus. *Q. J. Roy. Meteorol. Soc*., **130**, 1407-22.

Kaiser, D.P. and Qian, Y. (2002). Decreasing trends in sunshine duration over China for 1954 – 1998: Indication of increased haze pollution? *Geophys. Res. Lett.,* **29**, 2042, doi:10.1029/ 2002GL016057.

Kaufman, Y.J. and Fraser, R.S. (1997). The effect of smoke particles on clouds and climate forcing. *Science*, **277**, 1636-1639.

Kiehl, J.T., Schneider, T.L., Rasch, P.J., Barth, M.C. and Wong, J. (2000). Radiative forcing due to sulfate aerosols from simulations with the NCAR Community climate model (CCM3). *J. Geophys. Res*, **105**, 1441-160.

Koch, D. and Hansen, J. (2005). Distant origins of Arctic soot: A Goddard Institute for Space

Studies ModelE experiment. *J. Geophys. Res*., **110**, D04204, doi:10.1029/2004JD005296.

Koch, D, Jacob, D., Tegen, I., Rind, D. and Chin, M. (1999). Tropospheric sulfur simulation and sulfate direct radiative forcing in the Goddard Institute for Space Studies general circulation model. *J. Geophys. Res*., **104**, 13791-13823.

Koch, D., Schmidt, G. and Field, C. (2006). Sulfur, sea salt and radionuclide aerosols in GISS ModelE GCM. *J. Geophys. Res.,* **111**, D06206, doi:10.1029/2004JD005550.

Koren, I, Kaufmann,Y.J., Remer, L.A. and Martins, J.V. (2004). Measurement of the effect of Amazon smoke on inhibition of cloud formation. *Science*, **303**, 1342-1345.

Lahav, R. and Rosenfeld, D. (2000). Microphysical characterization of the Israel clouds from aircraft and satellites. *13th Intl. Conf. On Clouds. Precip*., **Proc**.**2**, 732.

Lelieveld, J. et al. (2002). Global air pollution crossroads over the Mediterranean. *Science*, **298**, 794-799.

Lohmann, U., Feichter, J., Chuang, C.C. and Penner, J.E. (1999). Prediction of the number of cloud droplets in the ECHAM GCM. *J. Geophys. Res*., **104**, D8, 9169-9198.

Menon, S., Del Genio, A.D., Koch, D., and Tselioudis, G. (2002a). GCM simulations of the aerosol indirect effect: Sensitivity to cloud parameterization and aerosol burden. *J. Atmos. Sci*., **59**, 692-713.

Menon, S., Hansen, J., Nazarenko, L. and Luo, Y. (2002b). Climate effects of black carbon aerosols in China and India. *Science*, **297**, 2250-2253.

Menon, S., (2004). Current uncertainties in assessing aerosol effects on climate. *Ann. Rev. Environ*. *Resour*., **29**, 1-31.

Nober, F.J., Graf, H.-F. and Rosenfeld, D. (2003). Sensitivity of the global circulation to the suppression of precipitation by anthropogenic aerosols. *Glob. Planetary Change*, **37**, 57-80.

Pandithurai, G., Pinker, R.T., Takamura, T. and Devara, P.C.S. (2004). Aerosol radiative forcing over a tropical urban site in India. *Geophys. Res. Lettr*., **31**, L12107, doi:10.1029/2004GL019702.

Penner, J.E, Zhang, S.Y. and Chuang, C.C. (2003). Soot and smoke aerosol may not warm climate. *J. Geophys. Res*., **108**, 4657, doi:10.1029/2003JD003409.

Ramanathan, V., Crutzen, P.J., Lelieveld, J., et al. (2001). Indian Ocean Experiment: An integrated analysis of the climate forcing and effects of the great Indo-Asian haze. *J. Geophys. Res*., **106**, 28371-28398.

Rinke, A., Dethloff, K. and Fortmann, M. (2004). Regional climate effects of Arctic haze. *Geophys. Res. Lettr.,* **31**, L16202, doi:10.1029/2004GL020318.

Roberts, D.L. and Jones, A. (2004). Climate sensitivity to black carbon aerosols from fossil fuel combustion. *J. Geophys. Res.,* **109**, D16202, doi:10.1029/2004JD004676.

Rudich, Y., Sagi, A. and Rosenfeld, D. (2003). Influence of the Kuwait oil fire plumes (1991) on the microphysical development of clouds. *J. Geophys. Res*., **108**, D15, doi:10.1029/2003JD003472.

Schmidt, G. A. et al. (2005). Present day atmospheric simulations using GISS ModelE: Comparison to in-situ, satellite and reanalysis data. *J. Clim.*, **19**, 153-192.

Twomey, S. (1977). The influence of pollution on the shortwave albedo of clouds. *J. Atmos. Sci.*, **34,** 1149-1152.

Van der Werf, G.R., Randerson, J.T., Collatz, G.J., Giglio, L., Kasibhatla, P.S., Arellano, A.F., Olsen, S.C. and Kasischke, E.S. (2004). Continental-scale partitioning of fire emissions during the 1997 to 2001 El Nino/La Nina period. *Science*, **303**, 73-76.

Wang, C. (2004). A modeling study on the climate impacts of black carbon aerosols. *J. Geophys*. *Res*., **109**, D03106, doi:10.1029/2003JD004084.

Wild, M., Ohmura, A., Gilgen, H. and Rosenfeld, D. (2004). On the consistency of trends in radiation and temperature records and implications for the global hydrological cycle. *Geophys. Res. Lettr*., **31**, L1201, doi:10.1029/2003GL019188.

Xu, Q. (2001). Abrupt change of the mid-summer climate in central east China by the influence of atmospheric pollution. *Atmos. Environ*, **35**, 5029-5040.

Table 3.1 Model simulations and their description.

Simulation	Type
Exp A	Standard run with both types of aerosol indirect effects
Exp A_S	Like Exp A but with changes to the aerosol burden (2x anthropogenic sulfate and 10% less biomass aerosols)
Exp NBC	Like Exp A but without any fossil- and biofuel sources for BC
Exp 2BC	Like Exp A but with twice the fossil- and biofuel sources for BC
Exp CC1	Like Exp A but including aerosol effects on convective clouds
Exp CC2	Like Exp CC1 but with a different treatment for determining cloud droplet number concentration in convective clouds
Exp NIE	Like Exp A but with fixed cloud droplet number

Table 3.2 Globally averaged annual values of aerosol column burdens (mg m^{-2}) for the different simulations. Two values listed for M02 are for 2 sets of simulations of the first and second indirect effects that mainly differ in the treatment of the autoconversion scheme. The values separated by '/' are for present-day and pre-industrial aerosol burdens. Note that in M02 only total organic aerosol burden was available that includes the biomass/terpene components.

Case	Sulfate Total	OC (fossil- & biofuel)	OC (biomass & terpene)	BC (fossil- & biofuel)	BC (biomass)	Net Cloud forcing (W m^{-2})
M02	2.66/0.42	1.57/0.14		-	-	–4.36
	5.03/1.05	2.46/0.27		-	-	–2.41
Exp A	2.96/0.15	0.98/0.57	1.61/0.80	0.13/0.0	0.12/0.06	–0.65
Exp A_S	4.34/0.14	0.96/0.55	1.63/0.15	0.12/0.0	0.12/0.01	–1.03

Table 3.3 Values of direct forcing and forcing efficiencies for the different species for Exp A.

Case	Sulfate Total	OC (fossil- and bio fuel, biomass)	BC (fossil- and biofuel)	BC (biomass)	Total
Direct forcing ($W\ m^{-2}$)	–0.29	–0.13	0.18	0.06	–0.18
Forcing efficiency ($W\ g^{-1}$)	–103	–106	1385	857	NA

Table 3.4a Simulated changes in the top of the atmosphere (TOA), surface, and atmospheric net radiation budgets ($W\ m^{-2}$), and precipitation over India/Indian Ocean region.

Indian Ocean (Jan-Mar) 0-20N, 40-100E	ΔTOA ($W\ m^{-2}$)	ΔSfc, ($W\ m^{-2}$)	ΔAtmos. ($W\ m^{-2}$)	Δ Prec (mm/d)
Exp A	–2.97	–7.33	4.36	0.35
Exp NBC	–2.07	–3.52	1.45	–0.08
Exp 2BC	–2.06	–5.71	3.65	0.01

Table 3.4b Similar to Table 3.4a but for differences over northern and southern China.

China (Jun-Aug) 90-120E		ΔTOA ($W\ m^{-2}$)	ΔSfc. ($W\ m^{-2}$)	ΔAtmos. ($W\ m^{-2}$)	Δ Prec. (mm/d)
Exp A	34-42N	–6.46	–5.38	–1.08	–0.39
	18-30N	–5.69	–7.77	2.08	0.05
Exp NBC	34-42N	–7.81	–5.17	–2.64	–0.10
	18-30N	–6.56	–6.90	0.34	0.24
Exp 2BC	34-42N	–3.87	–6.48	2.61	–0.77
	18-30N	–5.41	–9.28	3.87	–0.13

Table 3.5a Local radiative forcings for different vertical aerosol distributions (Johnson et al. 2004).

Condition	Semi-direct effect ($W\ m^{-2}$)	Direct effect ($W\ m^{-2}$)
Absorbing aerosol in boundary layer	22.8	20.5
Absorbing aerosol in and above boundary layer	10.2	15.4
Absorbing aerosol above boundary layer	–9.5	0.7
Scattering aerosol above boundary layer	–0.1	–7.4

Table 3.5b Local radiative forcings for different vertical distribution of aerosols over China (18-50N, 90-130E). (Menon, 2004).

Condition	Semi-direct effect ($W\ m^{-2}$)	Direct effect ($W\ m^{-2}$)
Standard aerosol distribution	–5.39	5.82
All aerosols in first layer (0.42 km)	0.97	–0.06
All aerosols in fourth layer (3.8 km)	–5.74	8.37
All aerosols in seventh layer (10.5 km)	–19.8	15.3

List of Figures:

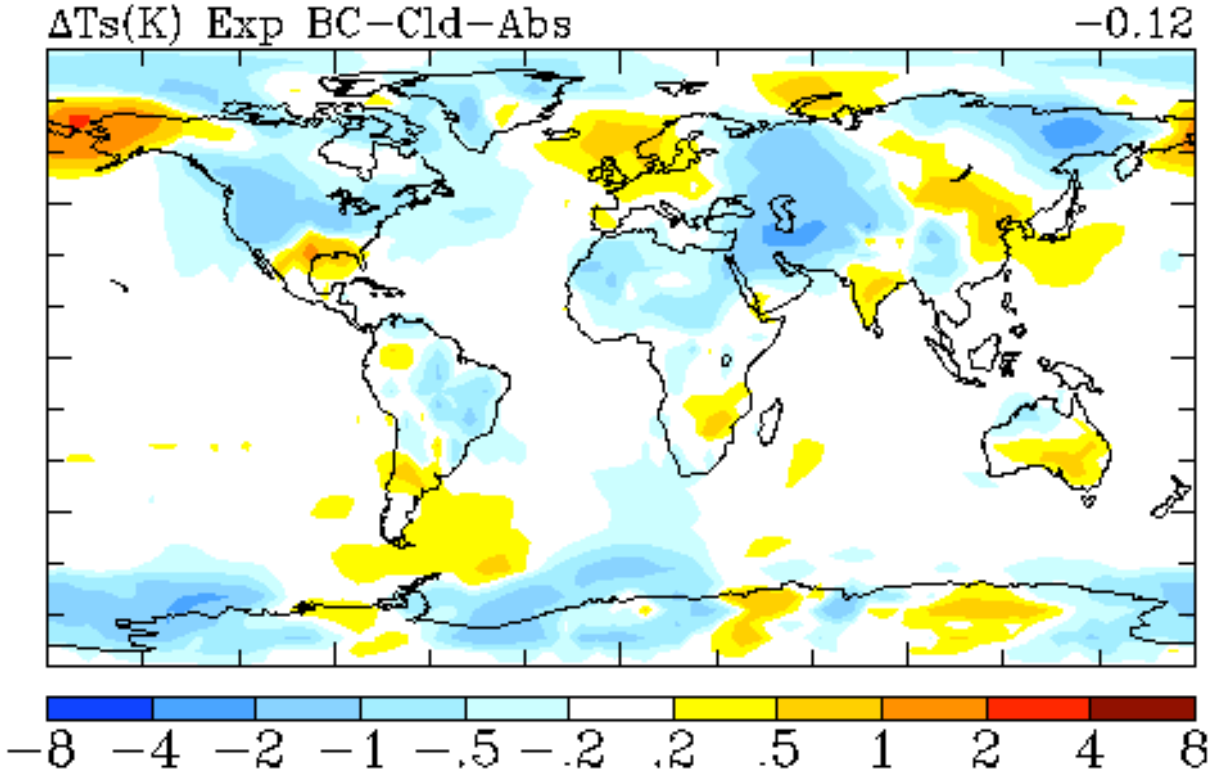
ΔTs(K) Exp BC−Cld−Abs
−0.12
−8 −4 −2 −1 −.5 −.2 .2 .5 1 2 4 8

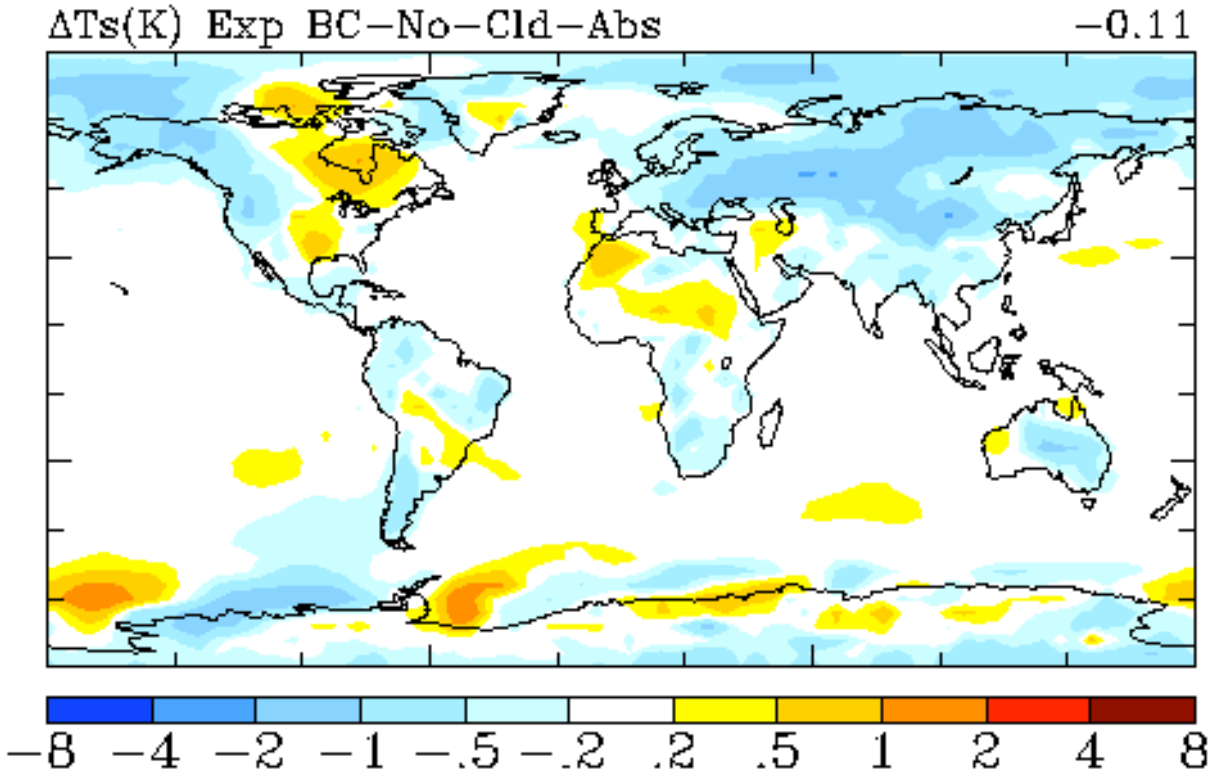
ΔTs(K) Exp BC−No−Cld−Abs
−0.11
−8 −4 −2 −1 −.5 −.2 .2 .5 1 2 4 8

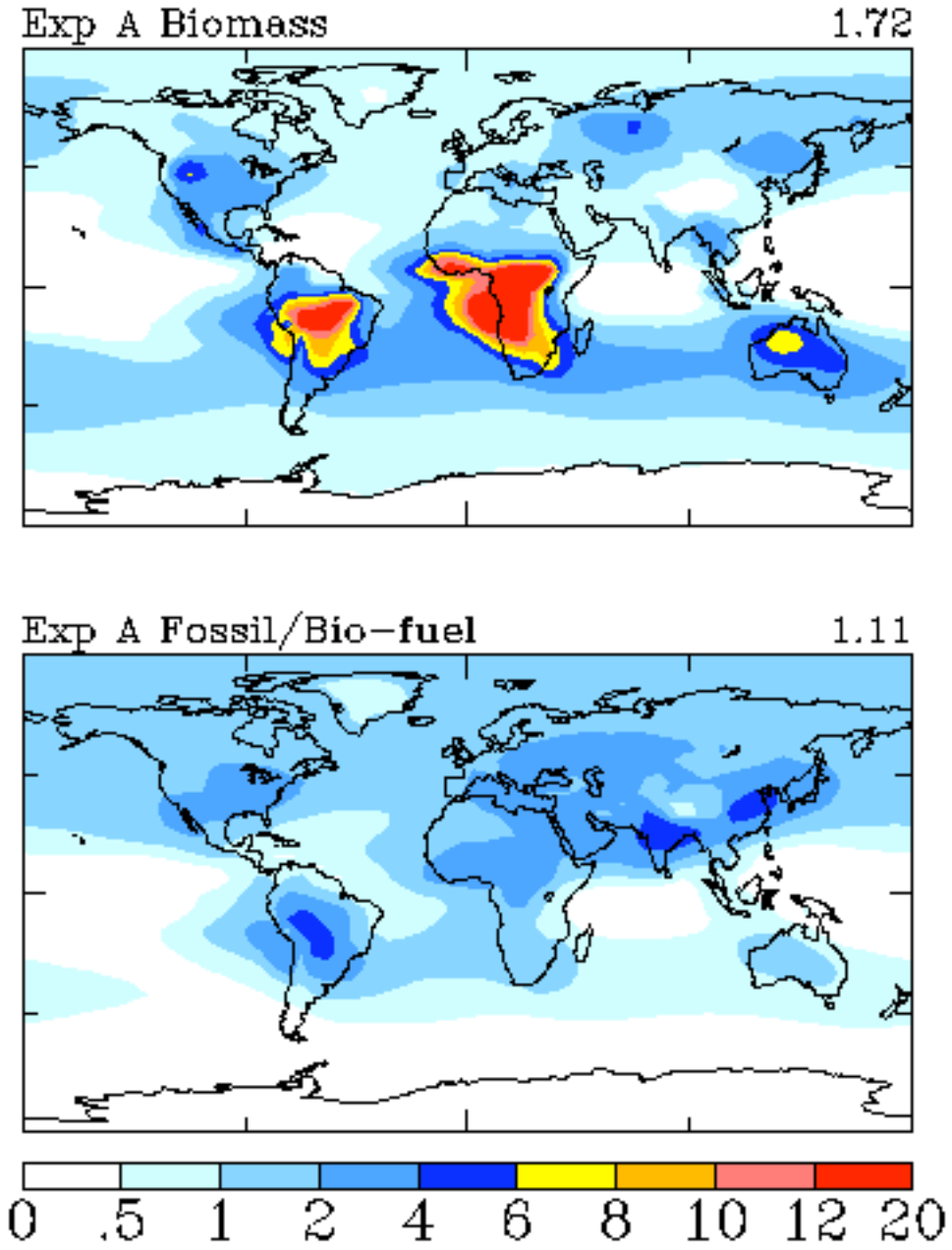
Exp A Biomass
1.72
Exp A Fossil/Bio-fuel
1.11
0 .5 1 2 4 6 8 10 12 20

a)

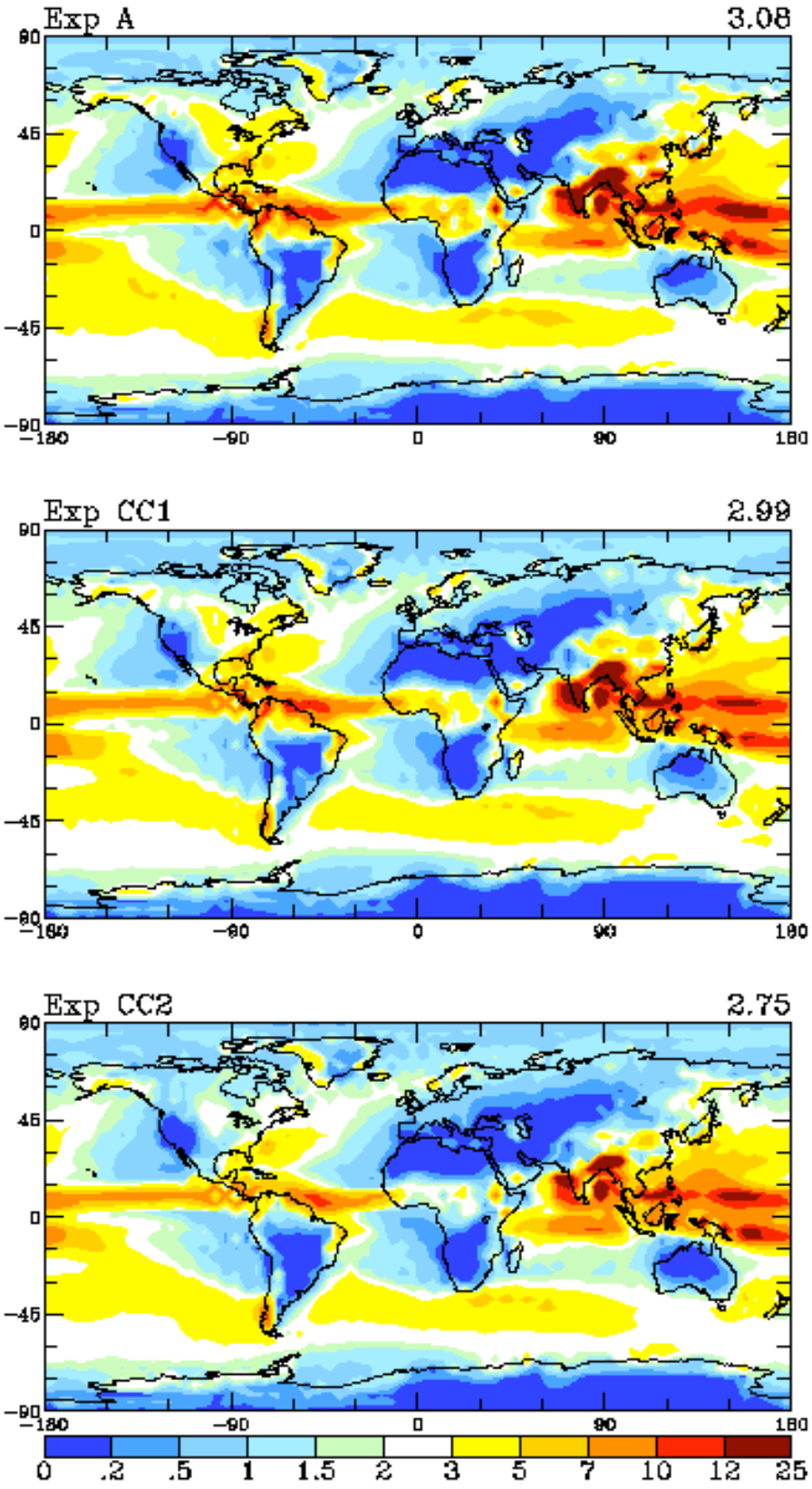
Exp A
3.08
Exp CC1
2.99
Exp CC2
2.75
90
45
0
-45
-90
-180
-90
0
90
180
0
.2
.5
1
1.5
2
3
5
7
10
12
25

b)

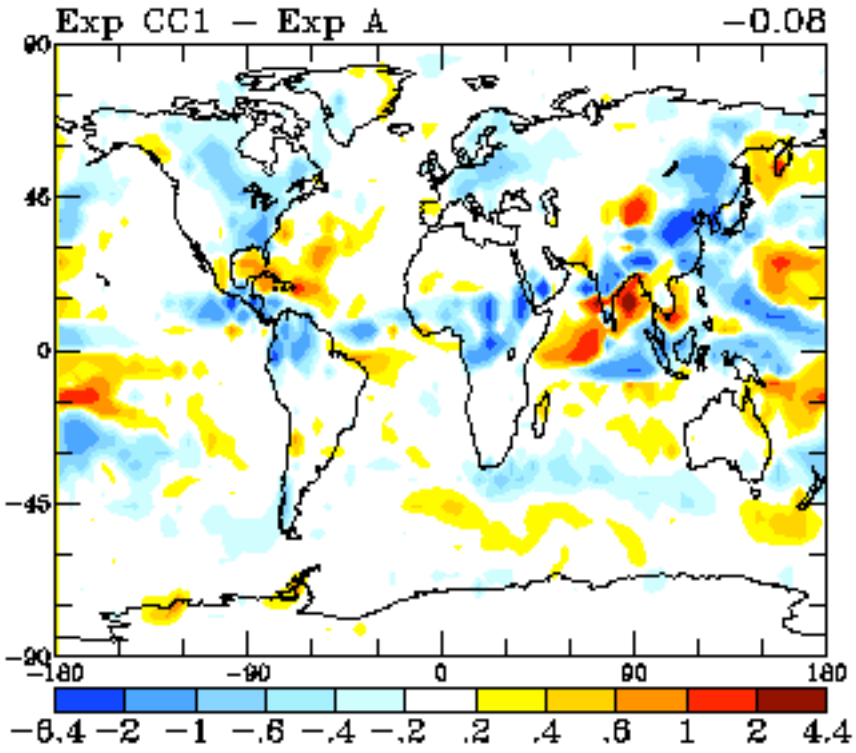

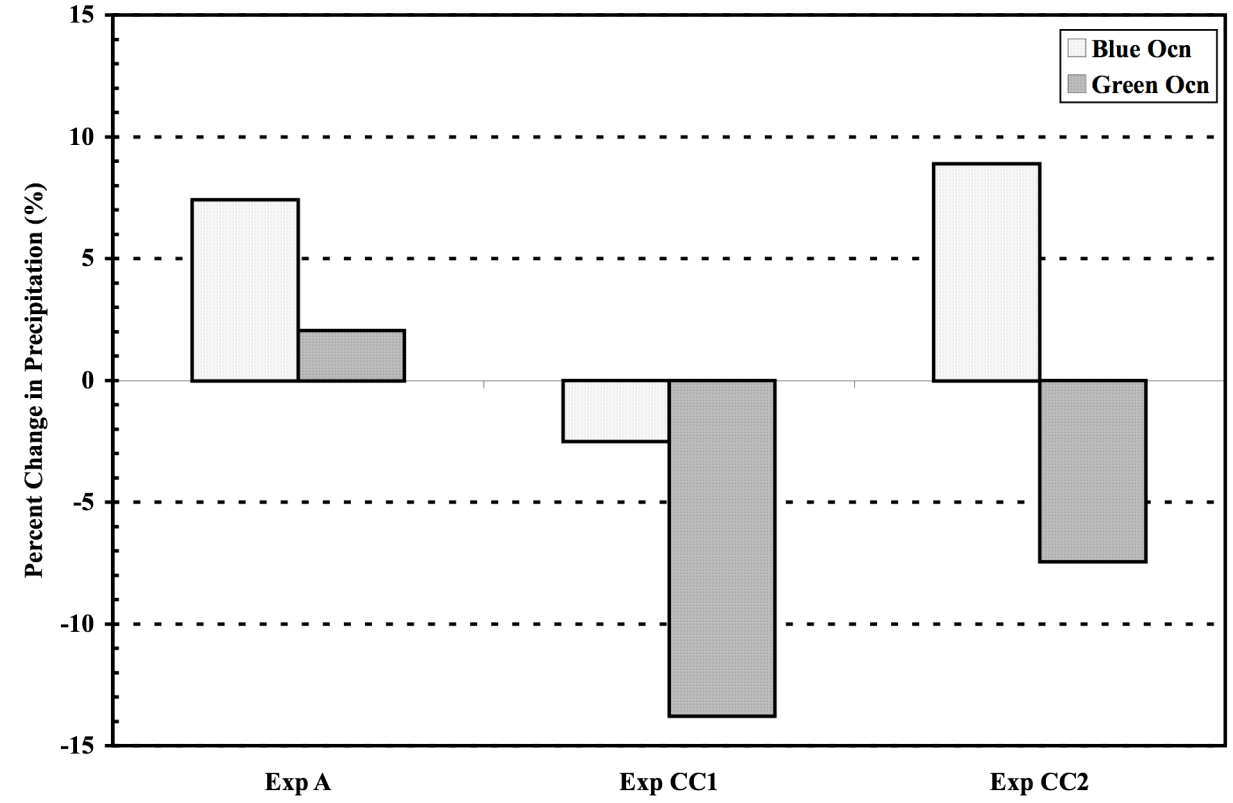
Blue Ocn
Green Ocn
Percent Change in Precipitation (%)
15
10
5
0
-5
-10
-15
Exp A
Exp CC1
Exp CC2

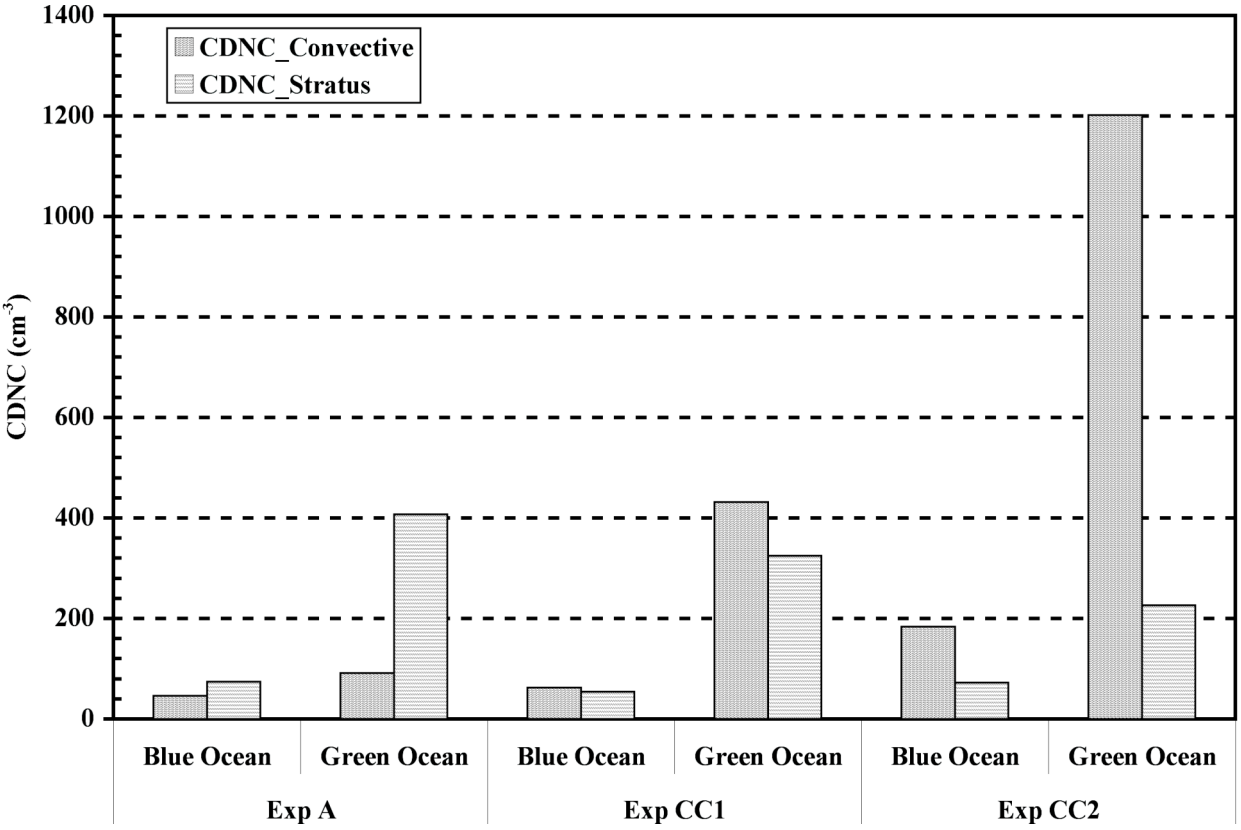
CDNC_Convective
CDNC_Stratus
CDNC (cm-3)
1400
1200
1000
800
600
400
200
0
Blue Ocean
Green Ocean
Blue Ocean
Green Ocean
Blue Ocean
Green Ocean
Exp A
Exp CC1
Exp CC2